
This is an electronic reprint of the original article.
This reprint may differ from the original in pagination and typographic detail.

Shen, Boxuan; Piskunen, Petteri; Nummelin, Sami; Liu, Qing; Kostiainen, Mauri A.; Linko, Veikko

Advanced DNA Nanopore Technologies

Published in:
ACS Applied Bio Materials

DOI:
[10.1021/acsabm.0c00879](https://doi.org/10.1021/acsabm.0c00879)

Published: 21/09/2020

Document Version
Publisher's PDF, also known as Version of record

Published under the following license:
CC BY

Please cite the original version:
Shen, B., Piskunen, P., Nummelin, S., Liu, Q., Kostiainen, M. A., & Linko, V. (2020). Advanced DNA Nanopore Technologies. *ACS Applied Bio Materials*, 3(9), 5606-5619. <https://doi.org/10.1021/acsabm.0c00879>

This material is protected by copyright and other intellectual property rights, and duplication or sale of all or part of any of the repository collections is not permitted, except that material may be duplicated by you for your research use or educational purposes in electronic or print form. You must obtain permission for any other use. Electronic or print copies may not be offered, whether for sale or otherwise to anyone who is not an authorised user.

Advanced DNA Nanopore Technologies

Boxuan Shen,[§] Petteri Piskunen,[§] Sami Nummelin, Qing Liu, Mauri A. Kostiaainen, and Veikko Linko*

Cite This: *ACS Appl. Bio Mater.* 2020, 3, 5606–5619

Read Online

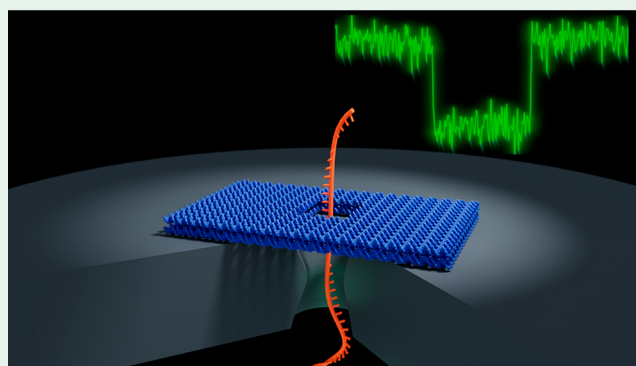
ACCESS |

Metrics & More

Article Recommendations

ABSTRACT: Diverse nanopore-based technologies have substantially expanded the toolbox for label-free single-molecule sensing and sequencing applications. Biological protein pores, lithographically fabricated solid-state and graphene nanopores, and hybrid pores are in widespread use and have proven to be feasible devices for detecting amino acids, polynucleotides, and their specific conformations. However, despite the indisputable and remarkable advantages in technological exploration and commercialization of such equipment, the commonly used methods may lack modularity and specificity in characterization of particular phenomena or in development of nanopore-based devices. In this review, we discuss DNA nanopore techniques that harness the extreme addressability, precision, and modularity of DNA nanostructures that can be incorporated as customized gates or plugs into for example lipid membranes, solid-state pores, and nanocapillaries, thus forming advanced hybrid instruments. In addition to these, there exist a number of diverse DNA-assisted nanopore-based detection and analysis methods. Here, we introduce different types of DNA nanostructure-based pore designs and their intriguing properties as well as summarize the extensive collection of current and future technologies and applications that can be realized through combining DNA nanotechnology with common nanopore approaches.

KEYWORDS: DNA nanotechnology, DNA origami, nanopore, sensing, sequencing, proteins



1. INTRODUCTION

Biological protein pores and pore-forming peptides have pivotal functions in cellular processes. They can act as regulators of molecular or ionic transport in response to external stimuli such as pH, voltage, and molecular binding. On the other hand, toxins, such as α -hemolysin and aerolysin, promote cell lysis by forming channels into lipid membranes and therefore interfere with the cellular osmotic balance.¹ In a technological viewpoint, various membrane-inserted biological nanopores (NPs) can be harnessed in sensing applications. Needless to say, there exist a plethora of other molecular channels that may be utilized in sensing applications, such as receptors and ligand-gated channels, but here the focus is on the discrete well-controlled pores that can be used as single sensing elements. By applying voltage across the membrane that separates the *cis* and *trans* electrode chambers of the instrument (Figure 1), the molecules translocate through the pore one by one and disturb the otherwise constant ionic current through the pore thus resulting in a measurable signal (resistive-pulse technique).² The same technique was employed already in the 1950s in detecting and counting bacteria from the solution,³ but the present-day nanoscopic pores provide such highly confined spaces that the properties of a single molecule can be analyzed in a straightforward manner. For example, α -hemolysin extracted from bacteria has

been widely used for nucleic acid analytics,⁴ and these protein NPs can also be utilized in sequencing of DNA strands⁵ using commercially available ready-to-use instrumentation.⁶

However, there exist many challenges in employing purely biological pores, rendering feasible artificial NP systems allowing customizable single-molecule detection and analytical capabilities highly desirable. An example of an artificial NP instrument contains liquid chambers divided by an insulating membrane with a lithographically engineered nanoscale opening through which the probed molecules are electrophoretically driven (see Figure 1a). These solid-state nanopores (SSNPs)⁷ are fabricated using standard lithographic top-down methods that offer mass-production possibilities, durability, and reasonable size and shape control. In addition, a graphene layer may act as an atomically thin and precise membrane for the pore device, thus serving as a robust alternative to other techniques while providing high resolution sequencing capability due to its unique electric properties.⁸

Received: July 15, 2020

Accepted: August 12, 2020

Published: August 12, 2020



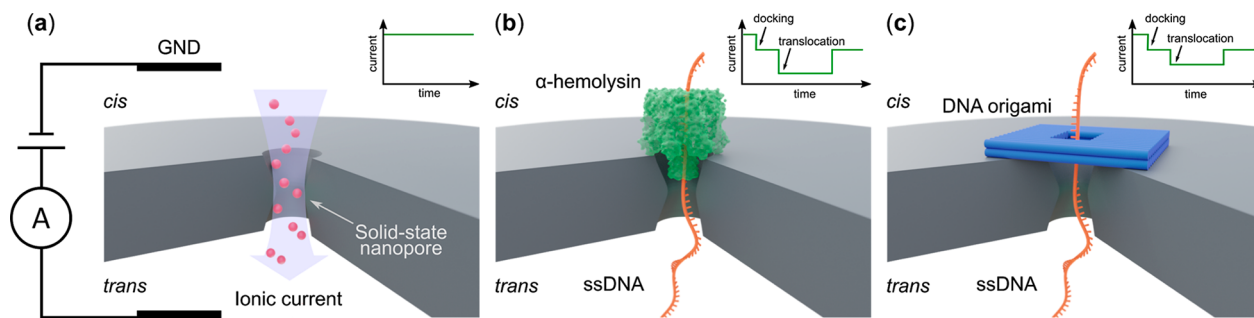


Figure 1. Various nanopore designs. The insets represent schematic single-channel current recordings (current vs time) in each case (signal shown in green). (a) Continuous ion current flows through solid-state nanopore (SSNP) due to the applied voltage across the membrane. GND denotes electrical ground. (b) α -Hemolysin protein pore is inserted into the SSNP where it can act as a gate for single-stranded DNA (ssDNA) translocation. (c) DNA origami is docked onto the SSNP where it can serve as a modular gatekeeper for a plethora of different uses.

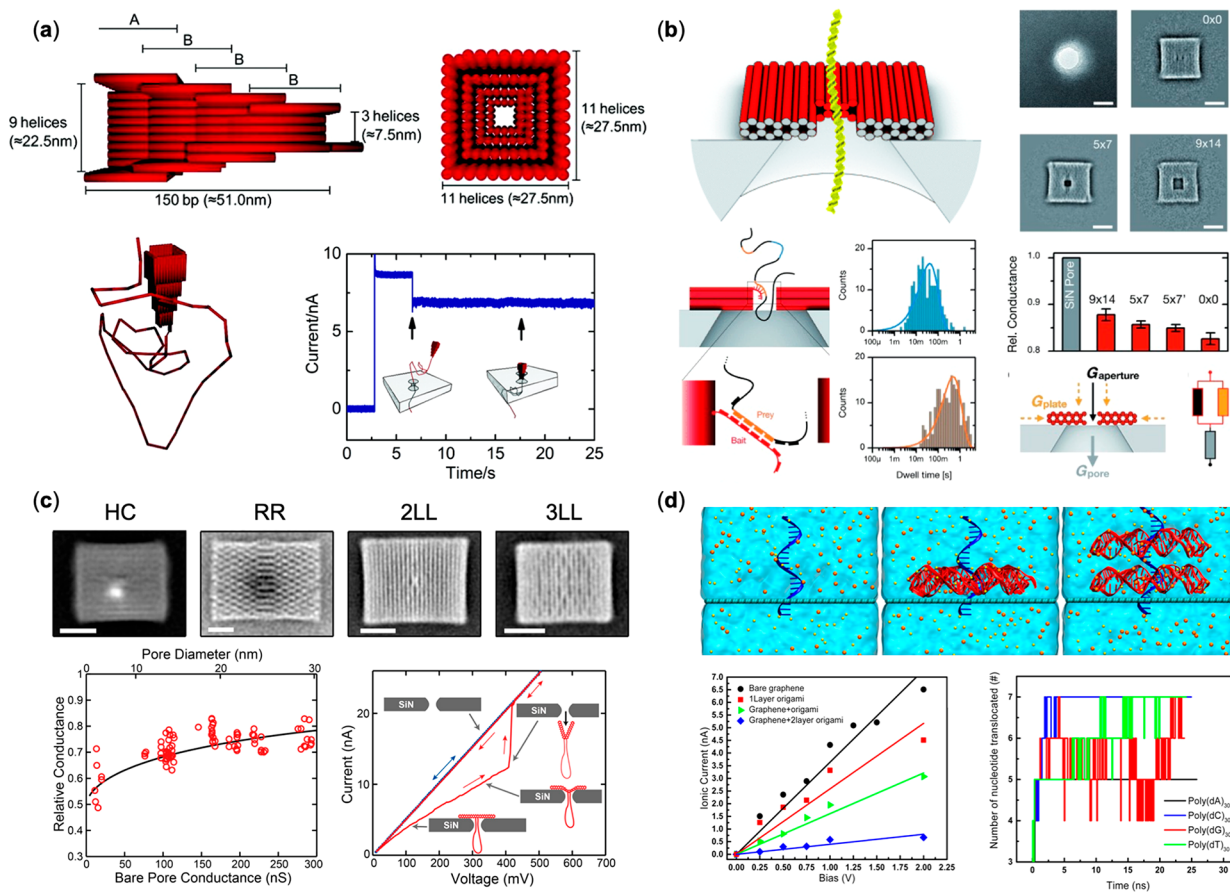


Figure 2. Hybrid NPs consist of DNA nanostructures and SSNPs in membranes. (a) Top panels: a funnel-like DNA nanostructure consists of 4 layers of DNA helices in a square lattice. Length $A = 40$ bp (13.6 nm), length $B = 48$ bp (16.3 nm). Bottom panels: a long dsDNA leash attached to the narrower end of the funnel pulls the DNA nanostructure into the SSNP when a negative voltage bias is applied, the insertion event is seen as the ionic current changes. (b) Top left panel: the model of a DNA strand translocating through a pore in a DNA nanoplate docked on top of a SSNP. Top right panel: transmission electron microscopy (TEM) images of a SSNP and DNA nanoplates with pores of different sizes. Bottom left panel: short unpaired ssDNA at the edge of the DNA NP forms a bait–prey system, which can influence the dwell time of the translocating long ssDNA depending on its sequence. Bottom right panel: relative conductance of DNA NPs with various sizes and electronic circuit model of the involved resistances. (c) Top panel: TEM class average images of four DNA origami nanoplates of different designs. HC, honeycomb lattice; RR, Rothemund rectangle; 2LL, 2 layer square lattice; 3LL, 3 layer square lattice. Bottom left panel: nonlinear fitting of the relative conductance versus bare pore conductance. Bottom right panel: plate buckling and pulling-through events reflected in ionic current changes. (d) Top panel: models of ssDNA molecules translocating through graphene NPs with 0, 1, or 2 layers of DNA origami. Bottom left panel: computational results of ionic current dependence of various combinations of graphene NP and DNA NP. Bottom right panel: computational simulation shows different dwell times of oligonucleotides with different sequences through a NP equipped with unpaired T bases at the pore edge. (a) Adapted from ref 38. Copyright 2012 American Chemical Society. (b) Adapted with permission from ref 39. Copyright 2012 WILEY-VCH Verlag GmbH and Co. KGaA, Weinheim. (c) Adapted from ref 40. Copyright 2014 American Chemical Society. (d) Adapted from ref 41. Copyright 2016 American Chemical Society.

However, the controllable chemical modification of these kinds of NPs is still challenging, although achievable through, for example, lipid coatings and polymer functionalization.^{9,10}

Alternatively, as mentioned above, the biological NPs that originally inspired solid-state pores already display highly complex gating behavior via the use of functional protein structures. If these proteins could be extracted and harnessed for use in man-made pores, biological pore functionality could very well be copied. Following this thought, eventually Hall and his co-workers¹¹ had the idea of mimicking a biological NP α -hemolysin and inserting it into a SSNP (Figure 1b), thus constituting the very first hybrid NP and thus paving the way for bridging top-down fabrication to atomically precise molecular self-assembly. Thus, hybrid NPs harnessed the excellent addressability and advanced functionality of biological macromolecules to provide SSNPs with the controllable chemical functionalization they were lacking.

In addition to employing ready proteins, lately also DNA-based nanotechnology has proven a popular method for functionalizing pores.^{12–15} In general, DNA nanotechnology allows fabrication of a variety of DNA objects with customizable size, shape, and modifications.¹⁶ Today, the emerged methods and techniques, including DNA origami,^{17–19} form an impressive toolbox for creating rather complex nanostructures^{20–22} for a wealth of diverse applications such as nanoelectronics,^{23–25} super-resolution imaging,²⁶ nanophotonics,²⁷ plasmonics,^{28–30} dynamic molecular robotics,^{31–33} molecular scale precision measurements,³⁴ and biomedicine.^{35–37} The possibility to engineer their properties, in particular the shape, confinement, and function, in an excellent precision has also made these shapes highly interesting in NP applications. As a step further from just mimicking nature as protein NPs do, tailored DNA structures provide a platform of fully addressable geometries, sensing-elements and moving parts, that allow users to design their own NP gates or even the pores themselves in a modular fashion (example of a DNA gatekeeper in Figure 1c).

In this review, we will discuss how exactly various DNA-based nanostructures have benefited the field of nanopore technologies. The review is divided into two main sections: DNA Nanostructure-Based Nanopores and Their Properties (Section 2), which details how DNA nanostructures have been harnessed for use in various types of conventional NPs (solid-state, capillary, lipid/vesicle), and Technologies and Applications (Section 3), where we discuss the more diverse DNA-based pore setups and their uses. In the latter section, we consider, for example, how a pore can be fashioned entirely of DNA nanostructures without a separate pore element, recent progress in DNA-assisted applied molecular detection and analysis technologies, as well as DNA NPs for digital data storage, and other intriguing applications.

2. DNA NANOSTRUCTURE-BASED NANOPORES AND THEIR PROPERTIES

2.1. DNA Nanostructures and Solid-State Nanopores.

The seminal work by Hall et al.¹¹ to combine α -hemolysin with artificial SSNPs has inspired the creation of hybrid DNA origami-based devices. Unlike α -hemolysin, which requires significant efforts to be modified by protein engineering to suit different applications, the excellent programmability and modularity of DNA nanostructures make it possible to fabricate NPs with fully customizable geometry and a variety of chemical modifications with ease. These benefits could

potentially complement SSNP features to facilitate more specific detection properties and a wider selection of analytes, for example, proteins in their natural conformations.

In 2012, Bell et al.³⁸ fabricated a funnel-shaped DNA origami structure with a 2344-base pair (bp) double-stranded DNA (dsDNA) leash, which facilitated the DNA origami to be inserted into a SSNP of 15 nm diameter in a SiN membrane to form a hybrid NP. The “funnel” consists of four layers of DNA helices in a square lattice geometry, with the openings of 22.5 nm (wider end) and 7.5 nm (narrower end) and a length of 51 nm (Figure 2a, top panels). The dsDNA leash (Figure 2a, bottom left panel) was formed by a part of the linearized scaffold strand hybridized to 49 complementary oligonucleotides. While applying a voltage across the SSNP with a solution of DNA nanostructure on one side, the funnels are driven by the ionic current flow and pulled by the leash until one of them is docked onto the solid-state pore, indicated by a sudden drop in the ionic current (Figure 2a, bottom right panel). In addition, the authors showed that by abruptly reversing the voltage applied, the origami could also be ejected from the pore. The insertion and ejection can be repeated several times providing a correction mechanism to replace a faulty origami pore. Finally, the authors demonstrated the sensing function of the assembled hybrid NP by successfully detecting translocation events of linearized λ -DNA.

In the same year, Wei et al.³⁹ assembled flat DNA origami plates in a honeycomb lattice with apertures of customizable sizes that acted as gatekeepers for SSNPs (Figure 2b). The authors characterized the electrical conductance of the DNA plate with and without apertures (Figure 2b, top right panel) when the plates were docked onto SSNP and showed that though a substantial leakage current and increased current fluctuations were present, the DNA nanoplate was still capable to detect the translocation events of biomacromolecules. By programming the dimensions of the aperture, the nanoplate worked as a filter for macromolecules with selected sizes. The nanoplates with $9 \times 14 \text{ nm}^2$ aperture allowed the smaller streptavidin to pass through but blocked the larger immunoglobulin G (IgG). The translocation events of long dsDNA of 6000 bp were also observed with an opening of $5 \times 7 \text{ nm}^2$. In addition, the authors demonstrated the effect of chemical modifications on the translocation behavior of molecules. By attaching a bait (short sequences for a DNA target) at the entrance of the gate, DNA molecules with varied lengths of sequences complementary to the bait showed different dwell times. This difference was reflected in the switching frequencies between two defined ionic current levels. Interestingly, the gatekeeper allowed analysis of phage plasmids with complicated secondary structures when the DNA plugin was equipped with multiple bait motifs. These results implied promising applications in biomolecular interaction screening and DNA sequence detection.

A more detailed study on ionic permeability of DNA origami nanoplates docked onto SSNPs was conducted by Plesa et al.⁴⁰ in 2014. As discussed in the earlier work,³⁹ the ionic current through a nanoplate is dependent both on the SSNP size and the nanoplate geometry. To better characterize the effect of the geometry of nanoplate, relative conductance (RC), that is, the ratio between the conductance of the hybrid pore and the SSNP ($RC = G_{\text{hybrid}}/G_{\text{pore}}$), was employed. Origami nanoplates with four different designs were compared, namely a honeycomb lattice (HC), a Rothmund rectangle (RR), a two-layered lattice (2LL), and a three-layer lattice (3LL)

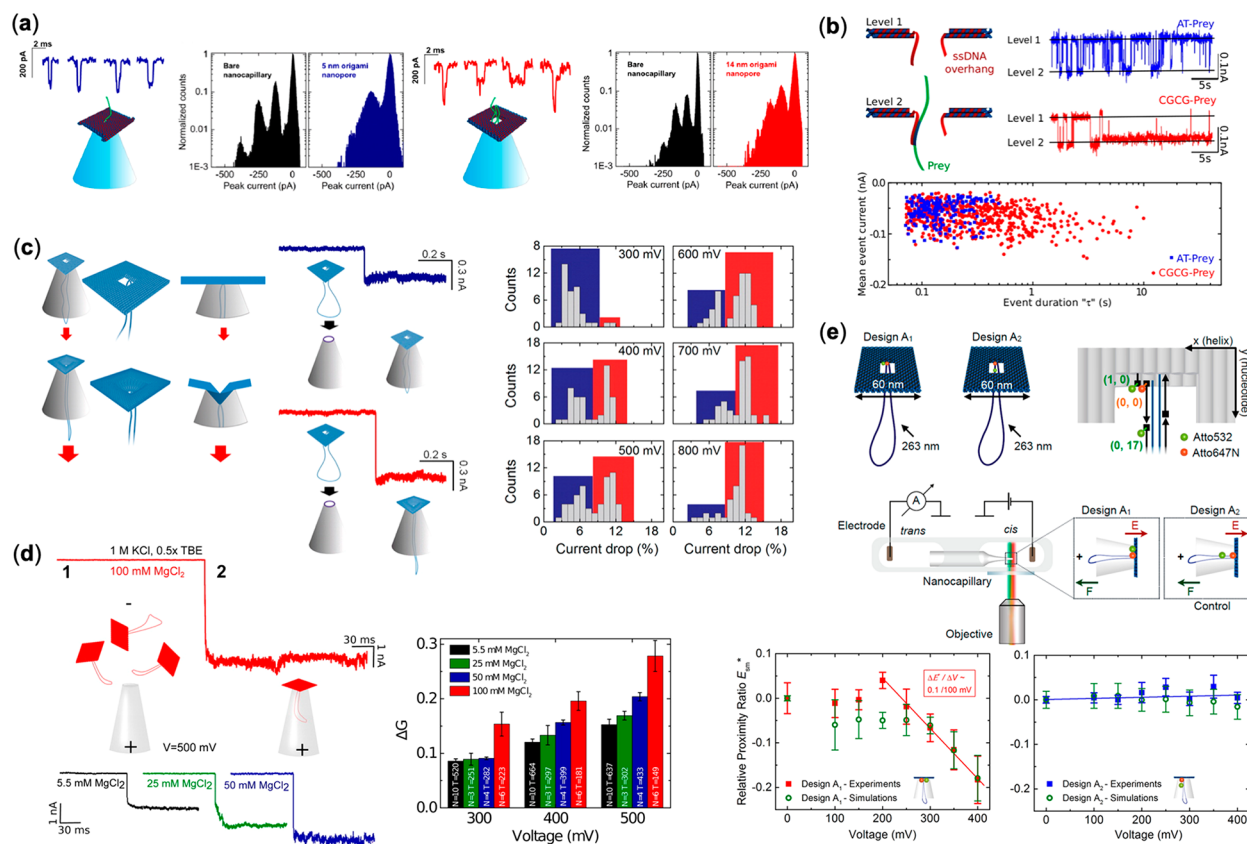


Figure 3. Deformable DNA nanostructures on nanocapillaries. (a) Representative current peaks during DNA translocation. Pore size can be used to limit possible folding conformations. (b) ssDNA overhangs can be extended around the pore to provide sequence specific transient binding and delay DNA translocation. A longer binding sequence leads to longer translocation event duration. (c) Left panel: the two DNA origami plate conformations. A higher bias voltage results in a buckled conformation for the plate. Middle panel: respective ionic current drops for the two conformations. A larger current drop occurs in the buckled state. Right panel: histograms of the percentage drop in ionic current over different voltages. The system transitions toward higher current drops as the bias voltage is increased. (d) Left panel: trapping of DNA origami NP plates to nanocapillaries under different Mg²⁺ concentrations and the consequent drops in ionic current. Part 1 of the trace: ionic current flow through the bare nanocapillary. Part 2 of the trace: reduced ionic current level after the DNA origami plate is trapped. Right panel: the relative conductance change in respect to MgCl₂ concentration and applied bias voltage. A larger drop can be observed at higher voltages and Mg²⁺ levels. (e) Top panel: designs of the DNA origami plates for deformation based optical voltage sensing. Design A₁ has a FRET dye pair perpendicular to and design A₂ in parallel to the electric field. The nanocapillary system can thus be observed live with a fluorescent microscope. Bottom panel: experimental and simulation results for relative proximity ratios of the FRET dyes as a function of applied voltage. The fluorescence signal responds in the perpendicular design (A₁) as the distance between the dyes changes due to the origami deforming. (a, b) Reprinted from ref 44. Copyright 2013 American Chemical Society. (c) Reprinted from ref 46. Copyright 2014 American Chemical Society. (d) Reprinted from ref 47. Copyright 2015 American Chemical Society. (e) Adapted from ref 48. Copyright 2018 American Chemical Society.

(Figure 2c top panel). Counterintuitively, the HC showed the lowest leakage followed by the RR, while the thicker 2LL and 3LL turned out to be the most leaky ones. In addition, the RC is found to increase as the salt concentration in the buffer is decreased. Importantly, the bare pore conductance versus RC relation is not linear as described earlier by Wei et al.³⁹ (Figure 2c bottom left panel). Interestingly, the study also showed that the DNA origami nanoplates could be mechanically deformed and pulled through the SSNP when a sufficiently high voltage was applied (Figure 2c bottom right panel). Randomized sudden jumps of current between discrete levels were also observed and attributed to mechanical readjustments of the nanoplates. This work provided beneficial guidelines for DNA nanostructure design to optimize the electrical and mechanical performance of DNA NPs.

Besides SiN, a graphene sheet is another promising membrane candidate for SSNP because its single atomic thickness could potentially provide a higher signal resolution and signal-to-noise ratio. Although limited experimental work

has been demonstrated on DNA origami-graphene hybrid NPs, the computational study by Barati Farimani et al.⁴¹ for DNA detection has provided valuable information on such devices. In this study, zero, one, and two layers of DNA origami on top of a graphene sheet with a pore of 2.1 nm in diameter were simulated by molecular dynamics (MD) methods (Figure 2d, top panel), and the ionic current, conductance, and resistance were characterized. The translocation of a single-stranded DNA (ssDNA) through the hybrid pore was also studied, and the addition of origami pore could effectively slow down the translocation time and hence increase the signal resolution. Moreover, particular emphasis was placed on a bait-prey mechanism with unpaired T bases at the edge of the DNA origami pore for specific base pair interactions. The results showed that the bait sequence indeed created distinguishable dwell time for ssDNA with different sequences due to the hydrogen bond interaction (Figure 2d, bottom panel).

Recently, Ketterer et al.⁴² constructed a DNA origami ring with inner surface docked with intrinsically disordered proteins

(IDPs) known as FG-Nups, mimicking the nature-occurring gatekeeper, nuclear pore complex (NPC), for nuclear transport in eukaryotic cells. The authors attached the DNA rings onto SSNPs using the electrophoretic force and compared the ion conductance of 8 and 32 FG-Nups functionalized rings (8-NPS1 and 32-NPS1). They found the conductance blockade increased as the number of FG-Nups increased ($20 \pm 4\%$ for 8-NPS1 vs $35 \pm 5\%$ for 32-NPS1). Attachment of the mutated FG-Nup (8-NPS1-S and 32-NPS1-S) altered the current blockage ability ($18 \pm 3\%$ for 8-NPS1-S vs $31 \pm 10\%$ for 32-NPS1-S) due to the increased hydrophilicity of the protein assembly. Computer simulation of the system revealed ion conductance values that are well in line with experimental results. Thus, the reported platform is anticipated to serve as an ideal model for NPC study and sophisticated NPC mimics construction. Coincidentally, another group of researchers published a very similar design of DNA origami NPCs for studying IDPs; however, the main characterization method they employed was AFM, not ionic current.⁴³

2.2. DNA Nanostructures Inserted into Nanocapillaries. Well controlled nanoscale channels can also be made for example by laser-assisted pulling of pipet tips, thus easily fabricating an elongated SSNP. Such “nanocapillaries” offer a cost-effective alternative to the ordinary silicon based SSNPs, and they have thus found use as their own category of pore devices. In 2013, Hernández-Ainsa and co-workers⁴⁴ demonstrated how DNA origami could be reversibly attached to the openings of glass nanocapillaries providing them with both physical and chemical functionality. They trapped two different double-layered DNA origami plates ($60 \times 54 \text{ nm}^2$) with either a 5 nm or a 14 nm rectangular pore in their center to a pulled glass nanocapillary (outer diameter $46 \pm 9 \text{ nm}$) by using a positive bias voltage ($>300 \text{ mV}$) (Figure 3a). The trapping event and formation of the hybrid NP were identified by a drop in ionic current and an increase in current noise. The origami could then be reversibly detached hundreds of times by applying a large opposite bias (-1000 mV), reverting the ionic current to its initial state each time. The trapping was further confirmed by attaching fluorescent dye molecules to the edges of the DNA origami and optically observing the exact moments the hybrid pores were formed and the ionic current dropped. As for further functionality, by using different pore sizes, they showed it was possible to physically limit in what folding states λ -DNA was able to translocate. Then, to additionally provide chemical functionality to their capillaries, the authors extended two staple strands on the 14 nm DNA origami pore to form ssDNA overhangs with controlled sequences (Figure 3b). These overhangs functioned as binding sites for ssDNA analytes with complementary segments, significantly slowing translocation time for only matching samples. Furthermore, this delay could be increased by using a longer, complementary overhang and thus stronger binding. Later on, this same sequence-specific delaying effect has also been exploited without the accompanying DNA nanostructures by directly functionalizing bare glass nanocapillaries with covalently bound ssDNA bristles.⁴⁵

DNA plates and pores are not just structurally static, but they are affected and deformed by the hydrodynamic and electrostatic forces involved in NP applications as shown by Plesa et al.⁴⁰ In 2014, Hernández-Ainsa et al.⁴⁶ also demonstrated this in their work when they attached a plate-like DNA origami NP to a pulled glass nanocapillary. Their DNA origami, a $60 \times 54 \text{ nm}^2$ plate with a $14 \times 15 \text{ nm}^2$ pore

and a long dsDNA scaffold leash in its center (Figure 3c, left panel), was guided to a capillary opening by applying a set positive voltage (300–800 mV). They observed that depending on the used voltage, the ionic current through the nanocapillary changed gradually and that they could eventually achieve two distinct states. With a sufficiently high voltage, the electrostatic forces overcame the stiffness of the DNA origami and the plate deformed as it was partially dragged into the capillary, leading to the existence of both an initial (300 mV) and a buckled (800 mV) state for the system (Figure 3c middle and right panel). While a higher voltage resulted in a larger population of buckled plates, an excessively high voltage ($>1000 \text{ mV}$) resulted in the plates completely translocating through the capillary. Similarly as in their earlier study,⁴⁴ reversing the voltage (-1000 mV) allowed them to detach the DNA origami from the capillaries at will. When their system was tested with λ -DNA translocation, the translocation rate was an order of magnitude lower in the buckled state as in the initial state, and two orders of magnitude lower than for the bare glass capillary. Thus, their work displayed how the behavior of the pore could be changed between distinct modes by just adjusting an external field.

The above behavior was initially attributed to just changes in the DNA origami pore dimensions, but this investigation was much more thoroughly continued by Li et al.⁴⁷ They used molecular dynamics simulations supported by electric current measurements and Förster resonance energy transfer (FRET) markers to elucidate how plate-based DNA origami actually behave in NP applications. They studied the effects of applied voltage, number of layers, nucleobase composition, lattice type, helical orientation, and solution Mg^{2+} ion concentration have on the ionic conductivity and permeability of DNA origami plates both by simulating and with experiments (Figure 3d). For the experimental work, they used varying designs of poreless DNA origami plates attached to glass nanocapillaries with different applied bias voltages. The molecular dynamics simulation was performed for the same designs as both free-floating and capillary-supported structures with varying magnesium concentrations and bias voltages. FRET was used to experimentally monitor the packing effect of Mg^{2+} . Their core finding was that the density and thickness of the origami defines how permeable it is to ions. As such, factors that packed the origami more tightly (increasing Mg^{2+} concentration, bending or higher number of the plates, more compact base pairs (CG), honeycomb lattice) hindered the flow of ions in the system. Conversely, loose packing and density lowering factors (lower Mg^{2+} concentrations, minimal number of layers, plate separation due to strong electric fields, AT heavy nucleobase composition, and a square lattice) all notably increased ionic conductivity. Interestingly, while a stronger electric field separated plates and thus increased ionic conductivity in free-floating origami, those supported by a NP or capillary displayed a net decrease in conductivity due to deformation, similarly as had happened in the earlier work.⁴⁶ Li et al. also showed that the orientation of the helices respective to the applied voltage determined conductivity. By tethering cube-like DNA origami to a nanocapillary with the DNA helices both parallel and perpendicular to the voltage, they were able to show that directions parallel to the helices were more conductive. Overall, their exhaustive study showed how the ionic conductivity, and thus ultimately the leakage currents that partially define a NPs sensitivity, could be engineered by clever design of the DNA origami element, not just in

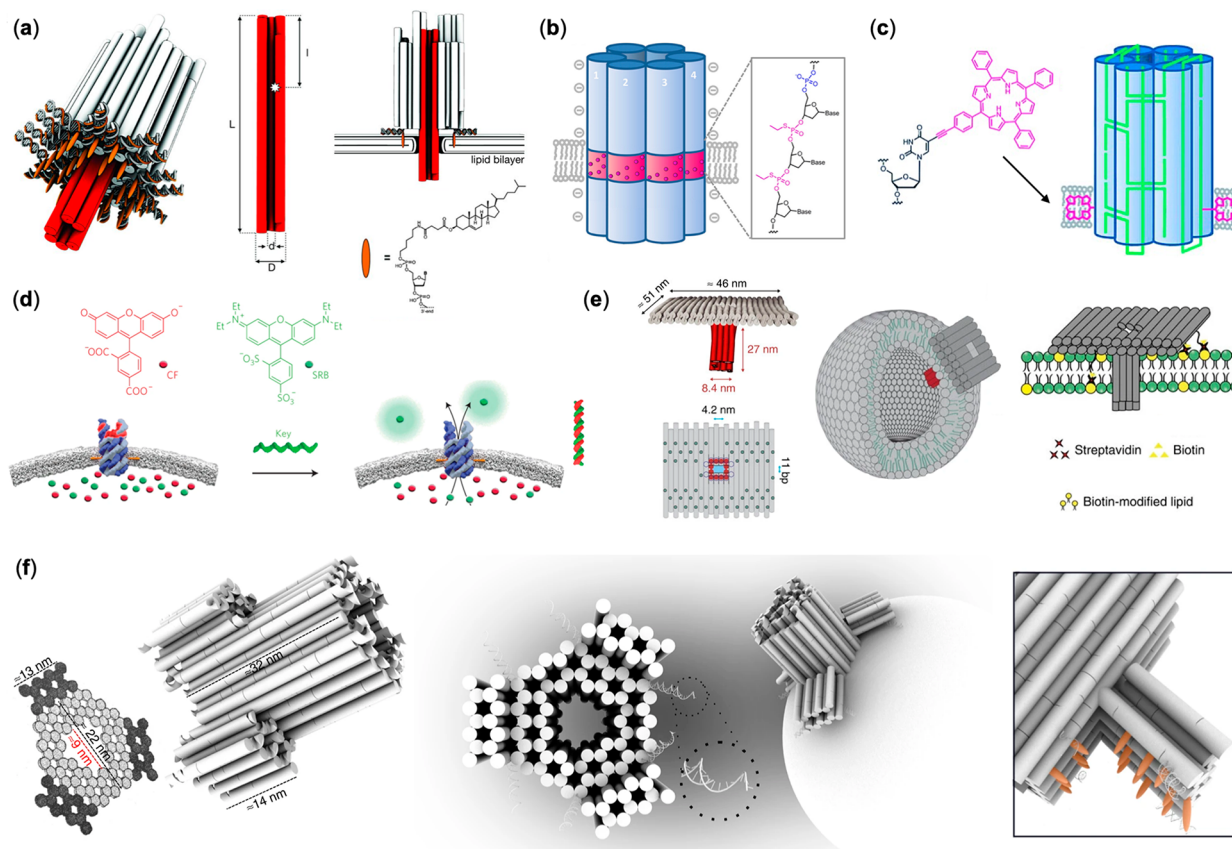


Figure 4. Synthetic DNA nanopore transmembrane channels. (a) 54HB stem having 26 cholesterol anchors (orange ellipsoids) with hollow inner channel (red cylinders) (left), geometric specifications of the transmembrane channel. Length $L = 47$ nm, tube diameter $D = 6$ nm, inner diameter $d = 2$ nm (middle), cross-sectional view of DNA barrel in a lipid bilayer (top right), chemical structure of cholesterol anchors (bottom right). (b) 15 nm long hexagonal 6HB barrel showing a membrane-spanning hydrophobic belt (magenta) with charge-neutral phosphorothioate-ethyl anchors (inset), (c) 6HB DNA NP design showing deoxyuridine attached to tetraphenylporphyrin (TPP) anchors via acetylene linkage at the 5 position of the nucleobase. (d) DNA-triggered (green strand) and charge-selective release of small-molecule cargo through a vesicle membrane wall. Fluorophore carboxy-fluorescein (red dots), sulforhodamine B (green dots), cholesterol lipid anchors (orange). (e) Design of the DNA T pore channel illustrating a side view (top left) and a top view (bottom left), schematic representation of a T pore embedded in a small unilamellar vesicle (middle), illustration of a membrane plate implantation via streptavidin–biotin bridges (right). (f) Side- and top-view of hexagonal pseudosymmetric DNA NP showing dimensions (left), schematic illustration of the NP embedded into a liposome via toehold mediated strand displacement opening of the flaps (middle), magnification of lipidated nucleic acid staples (orange ellipsoids) when flaps are in open form (right). (a) Reprinted with permission from ref 56. Copyright 2012 The American Association for the Advancement of Science. (b) Reprinted from ref 57. Copyright 2013 American Chemical Society. (c) Reprinted with permission from ref 59. Copyright 2013 The Authors. Published by Wiley-VCH Verlag GmbH and Co. KGaA. (d) Reprinted with permission from ref 64. Copyright 2016 Springer Nature Ltd. (e) Reprinted with permission from ref 65. Copyright 2016 Springer Nature Ltd. (f) Reprinted with permission from ref 67. Copyright 2019 Springer Nature Ltd.

nanocapillaries but also all other DNA origami-based NP applications.

As a display of how to exploit DNA origami for dynamic functionality, Hemmig et al.⁴⁸ later designed a nanocapillary hybrid system that was able to convert the deformation of the DNA origami pore element, and so the applied bias voltage, into quantized, fluorescent light. By using a leashed, two-layered plate-based design very similar as in ref 46 and attaching a FRET dye pair (Atto532 and Atto647N) to the pore opening, they were able to generate a fluorescent signal whose intensity depended on the state of the origami. The plates could then be attached to nanocapillaries in the same reversible way as demonstrated previously.⁴⁶ Now, as the emission intensity of the FRET pair is determined by the distance between the dye molecules and distorting the DNA origami changes this distance, the emission is thus affected by the applied voltage in the nanocapillary system. They used two configurations for the dyes: either perpendicular (~ 3 nm apart

in neighboring helices) or parallel (~ 5.8 nm apart along the leash strand) to the electric field (Figure 3e). First, coarse-grained Brownian dynamics simulations were used to test the designs, and the perpendicular alignment yielded a notable change in dye distance as a function of voltage, whereas the parallel alignment remained mostly unchanged. The plates were then experimentally tested by attaching them to quartz glass nanocapillaries (100–400 mV bias) and observing them with a fluorescence microscope capable of two-color alternating laser excitation (ALEX). Nearly as simulated, the perpendicular design was found to be sensitive to bias voltage changes between 200–400 mV, while the parallel design was not (Figure 3e, bottom panel). Thus, Hemmig et al. demonstrated how an optical voltage sensor could be set up from DNA origami attached to nanocapillaries.

2.3. DNA Nanopores for Lipid Membranes and Vesicles. The design and fabrication of membrane-penetrating NPs that can function as artificial channels are formidable

challenges owing to the entropic penalty associated with the insertion of synthetic pores into the hydrophobic domain of lipid membranes. Despite the challenges, NPs assembled from a variety of materials, including proteins, peptides, synthetic organic compounds, and DNA nanostructures, have been realized recently.⁴⁹ Because of the modularity of DNA nanostructures, their interactions with lipid membranes can be designed by attaching lipid modification at different locations. As a result, a plethora of lipid-interacting DNA nanostructures have been created,^{50,51} including DNA NPs with diversified sizes and shapes, from individual dsDNA molecules⁵² and DNA-tile assembled from eight oligonucleotides⁵³ to large DNA origami porins (up to ~ 6 nm in diameter) that allow transportation of folded proteins.^{54,55}

In 2012, Langecker et al.⁵⁶ first assembled nanometer-sized transmembrane channels into lipid bilayers by utilizing DNA origami honeycomb structures (Figure 4a). The synthetic channel structure was composed of two modules. One is a 54HB (HB = helix bundle) stem, where the six inner dsDNA helices were designed to function as a hollow channel that penetrate and span a lipid membrane. The other is a barrel-shaped cap having 26 covalently bound cholesterol units at the bottom to implant the structure to the *cis* side of the membrane. The assembly was evidenced by the marriage of small unilamellar vesicles (SUVs) made of POPC (1-palmitoyl-2-oleoyl-*sn*-glycero-3-phosphocholine) lipids and the orientation of DNA channels seen in transmission electron microscopy (TEM) images. This necessitates dynamic rearrangement of the lipid membrane around the DNA channel with the hydrophilic heads facing the charged stem of the structure, otherwise the assembly process would require substantial amounts of free energy (several 100 kJ mol^{-1}). Additional proofs of pore formation was provided by electrical measurements using a more stable DPhPC (1,2-diphytanoyl-*sn*-glycero-3-phosphocholine) bilayers that corroborated ion channel responses like those measured for natural ion channels, tunable gating behavior and single-molecule translocation which may enable, for example, sensing applications and interference with cellular homeostasis. Furthermore, the authors corroborated the ability of discrimination of single DNA molecules through pore translocation by following transient current blockades. By applying positive voltage bias, they demonstrated capture, unzipping, and subsequent translocation of a 9 bp DNA hairpin equipped with 50 Ts on the 3' end and 6 Ts on the 5' end, which was added to the *cis* side of the membrane. By reversing the bias, the translocated hairpin molecules could be transferred back to the *cis* side. In addition, they employed quadruplex-forming oligonucleotides with either a tail of 60 Ts or 125 deoxythymidines (dT), and followed the capture, threading, unfolding, and subsequent translocation of the molecules. Using the latter version of the quadruplex-forming molecule resulted in larger current blockades, which further emphasized the sensing capability of the developed pore system based on translocation characteristics.

Soon after, Burns and colleagues⁵⁷ introduced a related approach for the DNA pore formation in lipid membranes. A hexagonal 6HB barrel was composed of 15 nm duplexes, each substituted with charge-neutral phosphorothioate-ethyl (PPT) groups (12 PPT per duplex) in predefined positions. This ensures that a membrane-spanning hydrophobic ring is composed on the outer face of the hollow barrel to overcome energetic cost associated with the insertion of a DNA barrel into the hydrophobic environment of DPhPC lipid membrane

(Figure 4b). Insertion of the barrel was accomplished by applying alternate voltage in buffered media. NPs were proven structurally stable and generated a constant flow of ionic current through a single pore when 100 mV potential was applied. However, higher voltages up to 200 mV caused irreversible channel closure or the expulsion of pore from the membrane.

Redesigning the hollow 6HB barrel by moving the hydrophobic PPT-ring from center of the barrel to the bottom end enabled the membrane spanning pore formation and cytotoxic activity unlike three control structures that were not expected to bind SUV bilayers. Incubation with cervical cancer cells (HeLa) for 24 h at a concentration of $60 \mu\text{g mL}^{-1}$ (~ 100 nM concentration of NPs) decreased cell viability by 20%, except for controls. Confocal microscopy experiments corroborated that the pore-forming barrels were mainly located at the cellular membrane whereas the control structures, which did not contain a hydrophobic ring, were internalized. Thus, cytotoxic effect arises from a combination of DNA-pore formation and a hydrophobic ring that facilitate binding and interaction with cell membrane.⁵⁸

Burns et al.⁵⁹ presented an additional strategy where a 6HB DNA-NP was embedded to the giant unilamellar vesicles (GUVs) via porphyrin-based lipid anchors. Tetraphenylporphyrin (TPP) anchors were selected due to inherent hydrophobicity and fluorescence emission, which provided a practical tool to verify membrane anchoring (Figure 4c). 6HB was designed using caDNAno software⁶⁰ and assembled by annealing an equimolar mixture of four regular and two TPP-modified DNA strands. Insertion of the DNA-pores to micrometer-sized GUVs (prepared from DPhPC lipids using an electroformation unit) occurred via incubation in buffer medium at pH 8.0 and was confirmed by independent spectroscopic analysis based on the known fluorescence shift of porphyrin. Electric recordings, performed in nanocapillary to measure the ion flow across the lipid bilayers, yielded a distribution of conductances with a maximum of 250 picosiemens (pS). Because of the simplicity of the PPT version of the 6HB DNA-NP, its biophysical properties have been simulated with atomic precision.⁶¹ In addition, current-voltage (IV) characterization of the 6HB DNA-NP indicated that the pore could switch from a high-conductance (open) state to a low-conductance (close) state when a higher voltage bias was applied.⁶² The molecular mechanism of this voltage-switching behavior was later investigated computationally with MD simulations.⁶³ The simulations revealed that while the central tube lumen of the structure maintained a cylindrical shape, the mouth regions at the two termini undergo gating-like motions, causing temporal fluctuations in their aqueous volume, which presumably explains the lower conductance state of the NP.

Elaborated from the previous designs, Burns et al.⁶⁴ developed an elegant DNA NP equipped with hydrophobic cholesterol anchors, and a nanomechanical and sequence-specific gate to regulate transmembrane flux (Figure 4d). The DNA-barrel was redesigned to be shorter (~ 9 nm) than the previous ones (17–42 nm) to better match the thickness of DPhPC bilayer and thus regulate the flux of matter across the membrane. In addition, the 6HB design comprised concatenated DNA strands that combined two adjacent duplexes at their termini via single-stranded loops being simpler than traditional oligonucleotide connectivity. Closing of the nanomechanical gate was controlled by employing a “lock” strand

that formed a duplex with two docking sites close to the pore entrance. Opening of the gate was triggered by addition of a “key” strand that removed the lock via hybridization thus leaving the gate open. Single-channel current recordings for the open DNA NP depicted a steady current trace and conductance of 1.6 nS (on average) indicating stable pore formation across the lipid membrane. Closed form showed diminished flux (0.7 nS) suggesting minor ion permeability of the DNA pore wall or leakage from subnm gaps between the pore–lock assembly. Supplemental pore blockade experiments exploiting 14 poly(ethylene glycol) polymers (PEGs) of known hydrodynamic radius confirmed the expected 2.0 nm pore width since PEGs smaller than 1.8 nm migrated into the pore reducing its conductance, whereas larger PEGs did not. Moreover, the DNA pore was charge selective (Figure 4d) unlike natural protein pore α -hemolysin, allowing a positively charged small-molecule fluorophore sulforhodamine B (SRB) transport from lipid vesicles 13 \times faster than a negatively charged analog carboxy-fluorescein (CF).

In 2016, Krishnan et al.⁶⁵ presented a larger DNA-based pore with a \sim 4 nm diameter and simultaneously enhanced the anchor mechanisms of lipid adhering. The DNA membrane design was introduced as “DNA T pore” that comprised a double-layered DNA origami plate ($46 \times 51 \text{ nm}^2$) embedded with 12 helices forming a 27 nm hollow stem extending perpendicularly from the bottom of the origami plate as a transmembrane channel (inner cross-section $4.2 \times 4.2 \text{ nm}^2$). Down-side of the DNA origami plate was anchored via 57 hydrophobic tocopherol moieties facing to the SUV bilayer fabricated of POPC lipids (Figure 4e). For a comparison, a 6HB “pin” pore and a “wheel” pore analog (diameter \sim 2.6 nm, respectively) were constructed. In addition, an alternative strategy for membrane plate implantation was achieved by exploiting biotinylated lipids and streptavidin bridges on all three pore types (Figure 4e). Electrical measurements needed to corroborate pore formation was determined using the droplet interface bilayer (DIB) technique⁶⁶ exhibiting a conductance value of 3.1 nS for the T pore. Such large pores that can be inserted either an outside-in or an inside-out configuration enabled translocation events of ssDNA and dsDNA strands up to a length of 527 bp with increasing translocation speeds as a function of the transmembrane voltage. To further demonstrate the feasibility of the concept, three pores were incorporated into GUVs (mimics of artificial cells, diameter $>10 \mu\text{m}$), respectively, to perform dye influx experiments using fluorescent dye Atto 633 that does not penetrate the lipid membrane. The dye influx rates through DNA pores were monitored several hours using confocal laser fluorescence microscopy revealing dye influx induced by T pore and wheel pore, whereas the pin pore exhibited negligible influx due to poor penetration into the lipid membrane, which is consistent with electrical recordings.

To date, the largest synthetic transmembrane DNA NP has been presented by Thomsen et al.⁶⁷ who designed a 9.6 nm wide channel elaborated from a double layered pseudosymmetric hexagonal origami lattice having an outer diameter of 22 nm and a length of 32 nm (Figure 4f) measured from the negative-stain TEM images and single-particle 2D analysis. The dynamic NP design featured three programmable flaps that facilitated the insertion into SUVs made of POPC lipids. Each flap was locked in closed position by two staple strands respectively, to prevent aggregation induced by aqueous media. Flap opening via strand-displacement reactions exposed 46

nucleic acid strands decorated with 28 palmitoyl and 18 cholesterol moieties (Figure 4f inset) that, in turn, enhanced the penetration into the lipid membrane (Figure 4f). The opening of flaps was clearly visible on TEM images and Cy5–Cy3 FRET assays corroborated opening within minutes after addition of key strands. Total internal reflection fluorescence (TIRF) microscopy experiments enabled kinetic and thermodynamic studies of dye translocation. Surface immobilized SUVs loaded with Atto 655 dye were inserted with Atto 488-labeled preopened DNA pores, which facilitated real-time observation of NP docking time, reorientation time for pore insertion, ATTO 655 efflux rate, and subsequent comparison to α -hemolysin used as a positive control. The single-particle experiments revealed that the dye flux rate in α -hemolysin pores was dependent on the diameter of SUVs unlike in DNA pores. Size-selective gating of molecules was demonstrated with sulforhodamine B (SRB, 558 Da, $d \approx 0.5 \text{ nm}$), combined with a 40-kDa or a 500-kDa ($d \approx 4.8 \text{ nm}$ and $\approx 15.9 \text{ nm}$, respectively) dextran–FITC dyes employing a combination of surface-immobilized GUVs and Cy5-tagged DNA NPs. Dye influx was monitored 8 h using confocal laser scanning microscopy, which revealed rapid intake of SRB within GUVs. Translocation of the 40-kDa FITC dye was also successful, though much slower rate, whereas 500-kDa dye was too bulky to pass through the pore. Accordingly, the flux could be restricted by adding a molecular plug (ten 20-kDa PEG polymers, $d \approx 4.9 \text{ nm}$) within the DNA pore via available staple strand overhangs allowing translocation of small molecule SRB dye only. Moreover, the scope of size-specific cargo translocation properties was demonstrated by immobilized SUVs loaded with Atto 655 dye and 40-kDa dextran–tetramethylrhodamine (dTMR-40k). Subsequent DNA pore insertion permitted full efflux of the cargo while concise α -hemolysin pores used as a control, dTMR-40k remained encapsulated. Analogously, plugged DNA pores selectively allowed efflux of Atto 655 dye. Unplugging the pore by a toehold-mediated strand displacement mechanism released also the loaded dTMR-40k. Arguably, this concept may open up new avenues in many sensing applications.

The same 6HB pore design as in Figure 4d with three cholesterol lipid anchors (NP-3C) or without anchors (NP-0C, negative control) were employed to study structural, functional and thermal stability, and folding efficiency of DNA NPs in biological media.⁶⁸ In all, phosphate-buffered saline (PBS), bacterial growth medium lysogeny broth (LB), mammalian cell media Dulbecco’s modified Eagle medium (DMEM), and DMEM supplemented with 10% (v/v) fetal bovine serum (FBS) were investigated. In addition, counterion stabilization of NP-0C using Na^+ , K^+ and Mg^{2+} ions were explored. Just protein-containing FBS media showed complex formation with the DNA in sodium dodecyl sulfate polyacrylamide gel electrophoresis (SDS-PAGE). Thus, results imply efficient pore folding and high biocompatibility. Melting temperatures of the pore constructs were measured by FAM–Cy3 FRET pairs. In all media and salt conditions, melting transitions were well above physiological temperatures (45–54 $^\circ\text{C}$, respectively), even without the Mg^{2+} ions. Moreover, DNA NPs remained water-soluble in all buffer systems after 2 days, except in the presence of FBS, and were able to bind green fluorescence protein loaded GUVs verified by confocal laser scanning microscopy (CLSM) images. Nevertheless, it is noteworthy to mention that although the versatile pore system is compatible with various buffers and retains its functionality

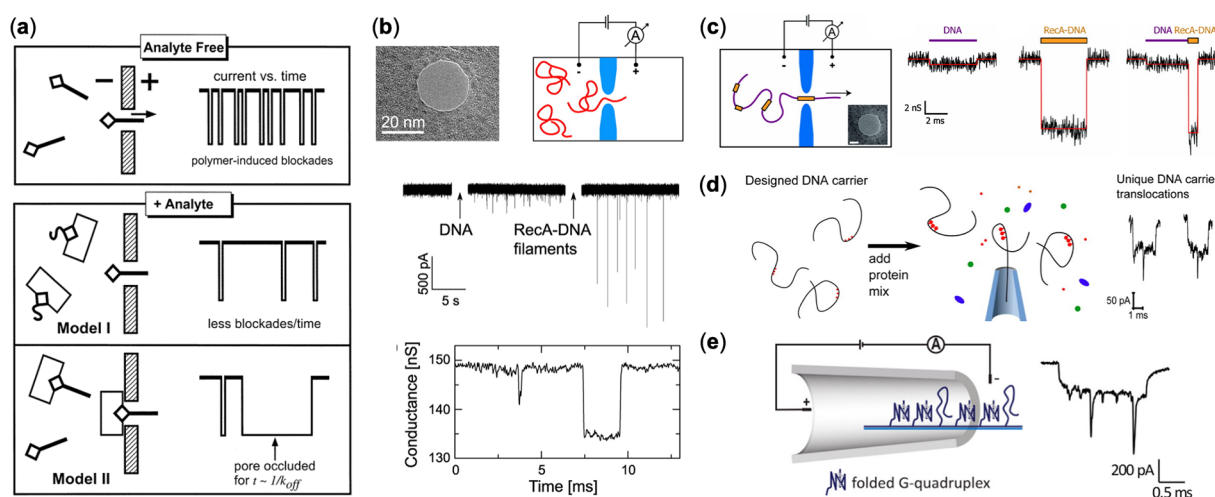


Figure 5. (a) Schematic illustration of the analytical sensor based on current blockades. (b) Top left panel: the TEM image of a NP. Top right panel: schematic illustration of the translocation of RecA-coated DNA. Middle panel: current recording before and after the addition of bare DNA and RecA-coated DNA. Bottom panel: two typical translocation events after addition of RecA-coated DNA. (c) Left panel: schematic illustration of the detection of RecA on dsDNA. Inset is a TEM image of the NP. Right panel: representation of current recording of typical translocation events for plain DNA, completely RecA-coated DNA and partially coated DNA. (d) Schematic overview of specific protein detection using designed DNA carriers. (e) Experimental setup of Gq NP assay and a typical current recording. (a) Reprinted from ref 73. Copyright 2001 American Chemical Society. (b) Reprinted from ref 76. Copyright 2009 American Chemical Society. (c) Reprinted from ref 77. Copyright 2010 American Chemical Society. (d) Reprinted from ref 82. Copyright 2015 American Chemical Society. (e) Reprinted from ref 84. Copyright 2019 American Chemical Society.

under different conditions, in serum-based and protein-rich solutions, such as in FBS, sensing and characterization of small analyte molecules becomes extremely complicated.

Very recently, Debnath et al.⁶⁹ showed that a DNA-based ionophore for preferential and stimuli-responsive K^+ transport across a biological membrane can be rationally assembled. The ionophore was formed using human telomeric G-quadruplex with noncovalently attached lipophilic guanosines, which facilitated the G-quadruplex anchoring to the hydrophobic lipid membrane. The authors deduced that the observed selective K^+ transport of the ionophore is due to the change of its conformation in response to different types of surrounding ions. Clearly, these results reinforce the suitability of advanced DNA nanotechnology as a versatile precision material for use in a plethora of biological studies such as specific targeting of cellular receptors and creating selective artificial transporters for diverse therapeutic and medical implementations.

As a final note to this section, while it is a common problem with many of the used anchoring modifications, chiefly cholesterol, that they tend to cause unwanted aggregation, it is also possible to control or exploit this behavior in the design of the DNA pores. For example, clever positioning of the lipid modifications can be used to deform and hydrophobically actuate (open/close) modified DNA structures on contact with surfactants and lipid bilayers,⁷⁰ or the modifications can be sterically hindered from forming aggregates with ssDNA overhangs that still allow the actual docking event to occur.⁷¹ For the interested reader, useful design rules were thoroughly investigated by Ohmann et al.⁷¹

3. TECHNOLOGIES AND APPLICATIONS

3.1. DNA-Assisted Methods for Molecular Detection and Analysis. The controlled design of DNA origami provides freedom in tuning of the pore size and shape, and thus, the customizable origami plugs could be employed in filtering of nano-objects, for example proteins in solution,

based on the size variation. This means that the hybrid device could be utilized for selecting, trapping or filtering certain molecules from the solution as explained above.³⁹ In addition, owing to its intrinsic anionic nature and outstanding addressability and programmability, DNA also presents an ideal analyte carrier, which hence greatly expands the application span of NPs. In this section, we will summarize recent advances in NP applications that are facilitated with DNA carriers. Early on, Kasianowicz et al. reported the transient current blockades in a single α -hemolysin channel caused by ssDNA and single-stranded RNA (ssRNA).^{4,72} Later, the same ion channel was applied for avidin detection with the help of biotinylated DNA polymers (Figure 5a).⁷³ The ion channel was reconstituted through the placement of a single α -hemolysin ion channel into a planar lipid bilayer. Subsequent addition of short or long biotinylated ssDNA and excess avidin resulted in two distinct current blockade models. Of particular interest is that this platform is able to measure the analyte concentration while maintaining excellent selectivity. Moreover, instead of linking recognition motif to a channel,⁷⁴ the as-reported method was based on rationally designed DNA sequences, which is more feasible and can eliminate concerns over complicated translocation induced by analyte mixture.⁷⁵

In contrast to the aforementioned method that monitored stochastic blocking events, Smeets et al. presented the first investigation on the translocations of DNA–protein structures through a SSNP (Figure 5b).⁷⁶ In this study, recombination protein A (RecA), which is known to form stable nucleoprotein filaments on dsDNA and facilitates homologous recombination and DNA repair, was first utilized to coat a 20 kbp dsDNA. Subsequent translocation measurements of dispersed analyte showed pronounced translocation time duration and conductance blockade compared to that obtained with native dsDNA. The nucleoprotein filament diameter was deduced from the conductance blockade, which fell well into the reported range. Besides, the results were confirmed by

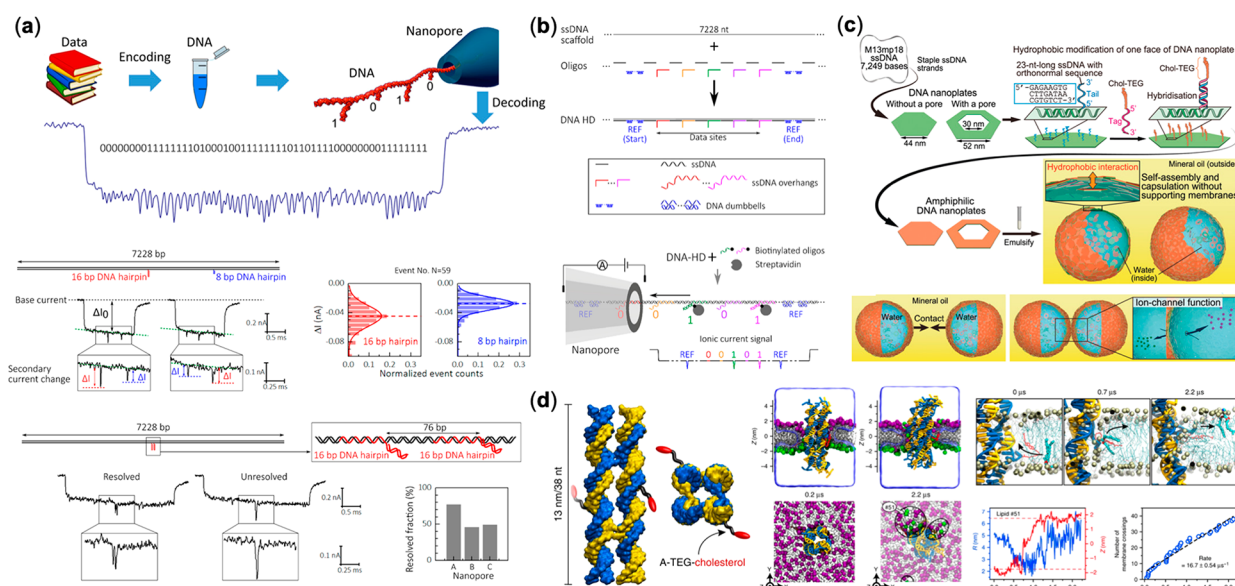


Figure 6. DNA-nanopore applications. (a) Digital information storage. Top panel: digital data is encoded into a linear DNA origami as 8 bp and 16 hairpins representing “0” bits and “1” bits, respectively. When the DNA information carrier translocates through a capillary NP, the data is decoded as current pulses of different depth. Middle panel: ionic current resolution test of hairpins. Bottom panel: spatial resolution test of hairpins 76 bp apart. (b) NP-based DNA hard drive. Top panel: ssDNA overhangs as data bits in a DNA-HD, bottom panel: biotinylated oligos conjugated with monovalent streptavidin hybridized to ssDNA overhangs as “1” bits. (c) Cholesterol-TEG modified amphiphilic DNA origami nanoplates stabilize water-in-oil nanodroplets. The NPs on the nanoplates function as ion channels which enable ion exchanges between nanodroplets in contact. (d) DNA scramblase. Left panel: side and top view of the model of TEG-cholesterol-modified DNA nanostructure. Middle panel: simulation shows the lipid (green and purple) exchange between the opposite leaflets of a lipid bilayer. Right top panel: time sequence of spontaneous interleaflet transfer of one lipid molecule (highlighted by the bold depiction) during a 2.2 μs MD simulation. Right bottom panel: radial distance relative to the center of mass of the nanostructure R (left axis) and the Z coordinate of the phosphorus atoms (right axis) of a lipid molecule and cumulative number of interleaflet transfer events (blue circles) vs. simulation time and its linear fit (dashed line). (a) Adapted from ref 86. Copyright 2019 American Chemical Society. (b) Reprinted from ref 87. Copyright 2020 American Chemical Society. (c) Reprinted with permission from ref 88. Copyright 2019 Wiley-VCH Verlag GmbH and Co. KGaA, Weinheim. (d) Adapted with permission from ref 89. Copyright 2018 Springer Nature Ltd.

rationaly placing the DNA–protein complex into the NP with the help of an optical tweezer. Enlightened by this observation, people from the same group sought the possibilities to identify the distribution of RecA on dsDNA (Figure 5c).⁷⁷ A 48.8 kbp dsDNA was first partially covered with RecA, forming uneven patchy RecA coatings along the dsDNA. Upon addition of the RecA-coated DNA to the NP, distinct translocation events were recorded, which was corresponding to size and distribution of coated RecA. Localization of RecA on dsDNA was resolved with a resolution of 8 nm, which corresponds to 5 RecA monomers binding to 15 bp of DNA. Later, they managed to detect single DNA-bound proteins at the single DNA molecule level, using phage DNA-binding antibodies as the model system.⁷⁸ On the other hand, Bulushev et al.⁷⁹ localized other DNA-binding proteins, *E. coli* RNA polymerase (RNAP) and dCas9, while Bell et al.⁸⁰ and Sze et al.⁸¹ realized multiplexed single-molecule protein screening along single DNA carrier.

Bell and Keyser⁸² expanded the concept by designing a DNA carrier for selective protein detection using glass NPs (Figure 5d). Protein translocation through NPs was measured in this study and the native state of proteins was preserved. In their design, the DNA carriers are composed of a linear DNA template that is modified at tailored positions for the binding of one or several proteins of interest. Using streptavidin as the model protein, they observed distinct current spikes close to the center of the translocation event. The detection sensitivity increased with the number of modified sites and the detectable current events reached $\sim 100\%$ when five biotins were attached

to the DNA carrier. It was also demonstrated that the DNA carrier was able to identify targeted protein against a background of protein mixture. As demonstrations of the adaptability of this method, they attached three biotin with ~ 600 nm intervals to the DNA carrier and three distinct current spikes at approximately equal time points were resolved, providing a feasible way for DNA velocity probing.⁸³ Moreover, the DNA carrier was proved to be sensitive in antibody detection when a digoxigenin was attached. Bošković et al.⁸⁴ utilized the same methodology to detect the formation and distribution of G-quadruplexes (Gq) along a single-stranded M13 DNA carrier using a single-molecule Gq NP assay (smGNA) (Figure 5e). Moreover, this assay revealed the Gq the formation kinetics in the presence of potassium and probed quadruplex-to-duplex structural transitions, demonstrating the feasibility over conventional label-requiring approaches which may disturb Gq formation.⁸⁵

3.2. Other Applications. A NP sensor translates the structural information on macromolecules into electric signals. By applying the same principle, Chen and co-workers⁸⁶ used NPs as high-resolution readout systems for digital data artificially stored in DNA nanocarriers. In their work, information was encoded in a linearized M13mp18 scaffold by a series of staples containing short hairpins. To decode the data, an integrated NP system that consists of a PDMS chip and capillary NPs with diameters of 5 nm was employed. When the nanocarriers translocate through the NP, the hairpin extrusions will cause a series of observable secondary ionic current pulses as readout. The current resolution of the system

was sufficient to distinguish hairpins of 8 bp from the ones of 16 bp, which represent “0” bits and “1” bits, respectively (Figure 6a). The spatial resolution has also been examined. With a 76-bp separation between the hairpins, 50% of the signals are still resolvable. However, to increase the accuracy, the actual encoding has spacers of 114 bp. The authors encoded 56 bits in a scaffold of 7,228 nt long. By analyzing tens of translocation events of such carriers by Bayesian inference method, 54 out of 56 bits were correctly read. Moreover, the data storage capacity can be further multiplied by connecting two scaffolds with a linker staple. This combination of programmability of DNA nanotechnology and the convenient conversion of a molecular structure feature to an electric signal by NP created a platform for digital data storage and extraction.

In 2020, Chen et al.⁸⁷ upgraded their research to the next level, in which the functions of a DNA hard-drive, including reading, writing, erasing, and rewriting, were realized. To enable these dynamic operations, several modifications to the system were made. First, instead of hairpins, biotinylated oligonucleotides and monovalent streptavidin were used to mark the “1” bit (Figure 6b). To erase the “1” bit, toe-hold based strand displacement was employed to release the biotinylated strand. Finally, to facilitate the smooth translocation of the nanocarrier with streptavidin, the diameter of the nanocapillary NPs were increased to 14 nm. Furthermore, to distinguish the direction of the nanocarrier translocation, asymmetric DNA dumbbells were placed at the beginning and end of the data bits as a reference signal (REF). The authors demonstrated the operations by writing a word in 5-bits ASCII code that represents “CAMBRIDGE” and rewriting it as “CAVENDISH”. Besides, an encryption method was also presented by withholding selected biotinylated strands as keys, the information can only be decrypted by physically restoring those bits with the correct keys.

Recently, research on DNA NPs modified with hydrophobic moieties revealed some of their intriguing properties, which may lead to unexpected applications. For example, Ishikawa et al.⁸⁸ in 2019 demonstrated a Pickering-like emulsion in which water-in-oil nanodroplets were stabilized by cholesterol-modified amphiphilic hexagonal DNA origami plates with pores (Figure 6c). Both fluorescence and ionic current measurements indicate that the designed NPs on the interfaces of the above-mentioned nanocapsules could function as channels to transport ions between nanodroplets in contact. Therefore, they may have applications in drug delivery and molecular robots.

Another interesting application of cholesterol-modified DNA nanostructures was presented by Ohmann et al.⁸⁹ who found that the DNA-tile NPs previously described by Göpfrich et al.⁵³ could catalyze spontaneous flipping of the lipid molecules between the two leaflets (Figure 6d). In other words, the cholesterol-modified DNA nanostructure has a similar function as a scramblase (a lipid flipping enzyme). The simulation indicates that such artificial scramblase could induce a lipid transfer rate up to 10^7 s^{-1} which is three orders of magnitude higher than its natural counterpart. Also, fluorescent experiments demonstrated that the DNA scramblase can mix the lipid composition on the opposite leaflets of a biological membrane both in vitro and in human cells, opening up possibilities for therapeutic applications.

4. CONCLUSIONS, CHALLENGES, AND PERSPECTIVES

In this review, we have discussed various DNA-based methods that can be combined with well-established high resolution, label-free, and single-molecule sensitivity enabling nanopore technologies. As explained here, DNA nanotechnology provides nearly arbitrarily shaped, spatially addressable and accurate DNA objects that can further act as modifiable plugins for solid-state nanopores or serve as pores themselves. Indeed, the straightforward and precise functionalization of DNA nanostructures makes them perfect candidates to achieve modulated translocation velocities and desired task-specific pore functions.

However, a plethora of challenges still remain. These include relatively high leakiness of the structures, gating effects, controlled orientation of the pore elements within a membrane, tendency of aggregation of functionalized pores especially the ones with tailored hydrophobic moieties such as cholesterol linkers and other amphiphilic modifications. In addition, there is an increasing interest toward employing nanopore systems for characterizing complex molecular reactions in a step-like manner. However, this is extremely difficult to achieve, as there are pragmatic restrictions such as signal-to-noise ratio and random blockade events that interfere with the analysis. Needless to say, due to the exact same reason, dissection of blockade events of small analyte molecules in biologically relevant media (for example serum-based buffers with high concentrations of proteins and protein aggregates) becomes arduous.

To tackle the other obstacles mentioned above, one can consider making use of a wealth of new design approaches and strategies. For example, in the case of undesired leakage current through the large DNA pores, the obvious problems are related to the mechanical stability of the pore structure. However, a straightforward method by Gerling et al.⁹⁰ to covalently cross-link the DNA strands provides mechanically and thermally stable structures through UV irradiation. To bring this sequence-programmable technique into practice, the same research group has further generalized the approach to create custom-sized, functional, and durable DNA origami structures.⁹¹ The other ways to achieve more robust structures are based on postfunctionalization strategies such as silicification^{92–94} of the DNA shapes or cross-linking⁹⁵ of the DNA-coating polymers.^{95,96} Moreover, the potentially achieved robustness of the DNA-based pores would also resolve the problem of using high bias voltages that are often required in electrical gating. On the other hand, stiffened or solidified structures may lack dynamic features that are needed in many biomedical approaches that rely on switching, actuation and conformational changes of the pore structure. Alas, so far these techniques have not been combined with the existing DNA nanopore methods; however, this work may already be underway while we are writing this.

Structural DNA nanotechnology has evolved significantly during the past two decades, and the reduced price of synthesis and biotechnological mass production possibilities for custom DNA structures⁹⁷ will further lower the barriers for their use in wide-range applications. Moreover, their feasibility can be further enhanced as there exist a plethora of methods to increase their stability for application-specific conditions.^{98,99} Nanopore technologies have likewise remarkably improved within a similar time window. As of today, the pore size can be

adjusted at the nanometer scale with state-of-the-art nano-engineering and the membrane thickness can reach the single-atom level (graphene pores), thus providing excellent signal resolution. Taking into account the rapid development within both research fields and the vast amount of examples provided through the fusion of these two, it is foreseeable that some DNA-based nanopore technologies can find uses in scientific exploration while others may be commercialized as extremely sensitive sensors for various analytes in, for example, personalized medicine. In addition, as there is an increasing interest toward employing DNA as a digital data storage, the methods allowing rapid reading of encoded information and using DNA-based nanopore devices as hard drives would provide intriguing solutions for recording, storing, and processing information in the near future.

AUTHOR INFORMATION

Corresponding Author

Veikko Linko – Biohybrid Materials, Department of Bioproducts and Biosystems and HYBER Centre, Department of Applied Physics, Aalto University, 00076 Aalto, Finland; orcid.org/0000-0003-2762-1555; Email: veikko.linko@aalto.fi

Authors

Boxuan Shen – Biohybrid Materials, Department of Bioproducts and Biosystems, Aalto University, 00076 Aalto, Finland

Petteri Piskunen – Biohybrid Materials, Department of Bioproducts and Biosystems, Aalto University, 00076 Aalto, Finland

Sami Nummelin – Biohybrid Materials, Department of Bioproducts and Biosystems, Aalto University, 00076 Aalto, Finland; orcid.org/0000-0003-2195-4818

Qing Liu – Biohybrid Materials, Department of Bioproducts and Biosystems and HYBER Centre, Department of Applied Physics, Aalto University, 00076 Aalto, Finland

Mauri A. Kostiainen – Biohybrid Materials, Department of Bioproducts and Biosystems and HYBER Centre, Department of Applied Physics, Aalto University, 00076 Aalto, Finland; orcid.org/0000-0002-8282-2379

Complete contact information is available at: <https://pubs.acs.org/10.1021/acsabm.0c00879>

Author Contributions

[§]B.S. and P.P. contributed equally.

Notes

The authors declare no competing financial interest.

ACKNOWLEDGMENTS

Financial support by the Emil Aaltonen Foundation, the Sigrid Jusélius Foundation, the Jane and Aatos Erkko Foundation, and the Vilho, Yrjö and Kalle Väisälä Foundation of the Finnish Academy of Science and Letters is gratefully acknowledged. This work was carried out under the Academy of Finland Centers of Excellence Programme (2014–2019).

REFERENCES

(1) Cao, C.; Long, Y.-T. Biological Nanopores: Confined Spaces for Electrochemical Single-Molecule Analysis. *Acc. Chem. Res.* **2018**, *51*, 331–341.
(2) Bayley, H.; Martin, C. R. Resistive-Pulse Sensing – from Microbes to Molecules. *Chem. Rev.* **2000**, *100*, 2575–2594.

(3) Kubitschek, H. E. Electronic Counting and Sizing of Bacteria. *Nature* **1958**, *182*, 234–235.
(4) Kasianowicz, J. J.; Brandin, E.; Branton, D.; Deamer, D. W. Characterization of Individual Polynucleotide Molecules Using a Membrane Channel. *Proc. Natl. Acad. Sci. U. S. A.* **1996**, *93*, 13770–13773.
(5) Wanunu, M. Nanopores: A Journey Towards DNA Sequencing. *Phys. Life Rev.* **2012**, *9*, 125–158.
(6) *Oxford Nanopore Technologies*; Oxford Nanopore Technologies, 2020. nanoporetech.com (accessed 07-15-2020).
(7) Dekker, C. Solid-State Nanopores. *Nat. Nanotechnol.* **2007**, *2*, 209–215.
(8) Garaj, S.; Hubbard, W.; Reina, A.; Kong, J.; Branton, D.; Golovchenko, J. A. Graphene as a Subnanometre Trans-Electrode Membrane. *Nature* **2010**, *467*, 190–193.
(9) Yusko, E. C.; Johnson, J. M.; Majd, S.; Prangko, P.; Rollings, R. C.; Li, J.; Yang, J.; Mayer, M. Controlling Protein Translocation Through Nanopores with Bio-Inspired Fluid Walls. *Nat. Nanotechnol.* **2011**, *6*, 253–260.
(10) Brilmayer, R.; Förster, C.; Zhao, L.; Andrieu-Brunsen, A. Recent Trends in Nanopore Polymer Functionalization. *Curr. Opin. Biotechnol.* **2020**, *63*, 200–209.
(11) Hall, A. R.; Scott, A.; Rotem, D.; Mehta, K. K.; Bayley, H.; Dekker, C. Hybrid Pore Formation by Directed Insertion of Alpha-Haemolysin into Solid-State Nanopores. *Nat. Nanotechnol.* **2010**, *5*, 874–877.
(12) Stoloff, D. H.; Wanunu, M. Recent Trends in Nanopores for Biotechnology. *Curr. Opin. Biotechnol.* **2013**, *24*, 699–704.
(13) Bell, N. A. W.; Keyser, U. F. Nanopores Formed by DNA Origami: A Review. *FEBS Lett.* **2014**, *588*, 3564–3570.
(14) Hernández-Ainsa, S.; Keyser, U. F. DNA Origami Nanopores: Developments, Challenges and Perspectives. *Nanoscale* **2014**, *6*, 14121–14132.
(15) Ding, T.; Yang, J.; Pan, V.; Zhao, N.; Lu, Z.; Ke, Y.; Zhang, C. DNA Nanotechnology Assisted Nanopore-Based Analysis. *Nucleic Acids Res.* **2020**, *48*, 2791–2806.
(16) Nummelin, S.; Kommeri, J.; Kostiainen, M. A.; Linko, V. Evolution of Structural DNA Nanotechnology. *Adv. Mater.* **2018**, *30*, 1703721.
(17) Rothmund, P. W. K. Folding DNA to Create Nanoscale Shapes and Patterns. *Nature* **2006**, *440*, 297–302.
(18) Douglas, S. M.; Dietz, H.; Liedl, T.; Högberg, B.; Graf, F.; Shih, W. M. Self-Assembly of DNA into Nanoscale Three-Dimensional Shapes. *Nature* **2009**, *459*, 414–418.
(19) Wang, P.; Meyer, T. A.; Pan, V.; Dutta, P. K.; Ke, Y. The Beauty and Utility of DNA Origami. *Chem.* **2017**, *2*, 359–382.
(20) Hong, F.; Zhang, F.; Liu, Y.; Yan, H. DNA Origami: Scaffolds for Creating Higher Order Structures. *Chem. Rev.* **2017**, *117*, 12584–12640.
(21) Julin, S.; Nummelin, S.; Kostiainen, M. A.; Linko, V. DNA Nanostructure-Directed Assembly of Metal Nanoparticle Superlattices. *J. Nanopart. Res.* **2018**, *20*, 119.
(22) Piskunen, P.; Nummelin, S.; Shen, B.; Kostiainen, M. A.; Linko, V. Increasing Complexity in Wireframe DNA Nanostructures. *Molecules* **2020**, *25*, 1823.
(23) Maune, H. T.; Han, S.-P.; Barish, R. D.; Bockrath, M.; Goddard, W. A., III; Rothmund, P. W. K.; Winfree, E. Self-Assembly of Carbon Nanotubes into Two-Dimensional Geometries Using DNA Origami Templates. *Nat. Nanotechnol.* **2010**, *5*, 61–64.
(24) Linko, V.; Paasonen, S.-T.; Leppiniemi, J.; Hytönen, V. P.; Toppari, J. J. Defined-Size DNA Triple Crossover Construct for Molecular Electronics: Modification, Positioning and Conductance Properties. *Nanotechnology* **2011**, *22*, 275610.
(25) Sun, W.; Shen, J.; Zhao, Z.; Arellano, N.; Rettner, C.; Tang, J.; Cao, T.; Zhou, Z.; Streit, J. K.; Fagan, J. A.; Schaus, T.; Zheng, M.; Han, S.-J.; Shih, W. M.; Maune, H. T.; Yin, P. Precise Pitch-Scaling of Carbon Nanotube Arrays within Three-Dimensional DNA Nanotrenches. *Science* **2020**, *368*, 874–877.

- (26) Graugnard, E.; Hughes, W. L.; Jungmann, R.; Kostiaainen, M. A.; Linko, V. Nanometrology and Super-Resolution Imaging with DNA. *MRS Bull.* **2017**, *42*, 951–959.
- (27) Gopinath, A.; Miyazono, F.; Faraon, A.; Rothmund, P. W. K. Engineering and Mapping Nanocavity Emission via Precision Placement of DNA Origami. *Nature* **2016**, *535*, 401–405.
- (28) Kuzyk, A.; Jungmann, R.; Acuna, G. P.; Liu, N. DNA Origami Route for Nanophotonics. *ACS Photonics* **2018**, *5*, 1151–1163.
- (29) Shen, B.; Kostiaainen, M. A.; Linko, V. DNA Origami Nanophotonics and Plasmonics at Interfaces. *Langmuir* **2018**, *34*, 14911–14920.
- (30) Shen, B.; Linko, V.; Tapio, K.; Pikker, S.; Lemma, T.; Gopinath, A.; Gothelf, K. V.; Kostiaainen, M. A.; Toppari, J. J. Plasmonic Nanostructures Through DNA-Assisted Lithography. *Sci. Adv.* **2018**, *4*, eaap8978.
- (31) Ijäs, H.; Nummelin, S.; Shen, B.; Kostiaainen, M. A.; Linko, V. Dynamic DNA Origami Devices: From Strand-Displacement Reactions to External-Stimuli Responsive Systems. *Int. J. Mol. Sci.* **2018**, *19*, 2114.
- (32) DeLuca, M.; Shi, Z.; Castro, C. E.; Arya, G. Dynamic DNA Nanotechnology: Toward Functional Nanoscale Devices. *Nanoscale Horiz.* **2020**, *5*, 182–201.
- (33) Nummelin, S.; Shen, B.; Piskunen, P.; Liu, Q.; Kostiaainen, M. A.; Linko, V. Robotic DNA Nanostructures. *ACS Synth. Biol.* **2020**, *9*, 1923–1940, DOI: 10.1021/acssynbio.0c00235.
- (34) Castro, C. E.; Dietz, H.; Högberg, B. DNA Origami Devices for Molecular-Scale Precision Measurements. *MRS Bull.* **2017**, *42*, 925–929.
- (35) Surana, S.; Shenoy, A. R.; Krishnan, Y. Designing DNA Nanodevices for Compatibility with the Immune System of Higher Organisms. *Nat. Nanotechnol.* **2015**, *10*, 741–747.
- (36) Ijäs, H.; Hakaste, I.; Shen, B.; Kostiaainen, M. A.; Linko, V. Reconfigurable DNA Origami Nanocapsule for pH-Controlled Encapsulation and Display of Cargo. *ACS Nano* **2019**, *13*, 5959–5967.
- (37) Keller, A.; Linko, V. Challenges and Perspectives of DNA Nanostructures in Biomedicine. *Angew. Chem., Int. Ed.* **2020**, DOI: DOI: 10.1002/anie.201916390.
- (38) Bell, N. A. W.; Engst, C. R.; Ablay, M.; Divitini, G.; Ducati, C.; Liedl, T.; Keyser, U. F. DNA Origami Nanopores. *Nano Lett.* **2012**, *12*, 512–517.
- (39) Wei, R.; Martin, T. G.; Rant, U.; Dietz, H. DNA Origami Gatekeepers for Solid-State Nanopores. *Angew. Chem., Int. Ed.* **2012**, *51*, 4864–4867.
- (40) Plesa, C.; Ananth, A. N.; Linko, V.; Gülcher, C.; Katan, A. J.; Dietz, H.; Dekker, C. Ionic Permeability and Mechanical Properties of DNA Origami Nanoplates on Solid-State Nanopores. *ACS Nano* **2014**, *8*, 35–43.
- (41) Barati Farimani, A.; Dibaeinia, P.; Aluru, N. R. DNA Origami–Graphene Hybrid Nanopore for DNA Detection. *ACS Appl. Mater. Interfaces* **2017**, *9*, 92–100.
- (42) Ketterer, P.; Ananth, A. N.; Laman Trip, D. S.; Mishra, A.; Bertolin, E.; Ganji, M.; van der Torre, J.; Onck, P.; Dietz, H.; Dekker, C. DNA Origami Scaffold for Studying Intrinsically Disordered Proteins of the Nuclear Pore Complex. *Nat. Commun.* **2018**, *9*, 902.
- (43) Fisher, P. D. E.; Shen, Q.; Akpinar, B.; Davis, L. K.; Chung, K. K. H.; Baddeley, D.; Sarić, A.; Melia, T. J.; Hoogenboom, B. W.; Lin, C.; Lusk, C. P. A Programmable DNA Origami Platform for Organizing Intrinsically Disordered Nucleoporins within Nanopore Confinement. *ACS Nano* **2018**, *12*, 1508–1518.
- (44) Hernández-Ainsa, S.; Bell, N. A.; Thacker, V. V.; Göpfrich, K.; Misiunas, K.; Fuentes-Perez, M. E.; Moreno-Herrero, F.; Keyser, U. F. DNA Origami Nanopores for Controlling DNA Translocation. *ACS Nano* **2013**, *7*, 6024–6030.
- (45) Youn, Y.; Lee, C.; Kim, J. H.; Chang, Y. W.; Kim, D. Y.; Yoo, K. H. Selective Detection of Single-Stranded DNA Molecules Using a Glass Nanocapillary Functionalized with DNA. *Anal. Chem.* **2016**, *88*, 688–694.
- (46) Hernández-Ainsa, S.; Misiunas, K.; Thacker, V. V.; Hemmig, E. A.; Keyser, U. F. Voltage-Dependent Properties of DNA Origami Nanopores. *Nano Lett.* **2014**, *14*, 1270–1274.
- (47) Li, C.-Y.; Hemmig, E. A.; Kong, J.; Yoo, J.; Hernández-Ainsa, S.; Keyser, U. F.; Aksimentiev, A. Ionic Conductivity, Structural Deformation, and Programmable Anisotropy of DNA Origami in Electric Field. *ACS Nano* **2015**, *9*, 1420–1433.
- (48) Hemmig, E. A.; Fitzgerald, C.; Maffeo, C.; Hecker, L.; Ochmann, S. E.; Aksimentiev, A.; Tinnfeld, P.; Keyser, U. F. Optical Voltage Sensing Using DNA Origami. *Nano Lett.* **2018**, *18*, 1962–1971.
- (49) Howorka, S. Building Membrane Nanopores. *Nat. Nanotechnol.* **2017**, *12*, 619–630.
- (50) Langecker, M.; Arnaut, V.; List, J.; Simmel, F. C. DNA Nanostructures Interacting with Lipid Bilayer Membranes. *Acc. Chem. Res.* **2014**, *47*, 1807–1815.
- (51) Birkholz, O.; Burns, J. R.; Richter, C. P.; Psathaki, O. E.; Howorka, S.; Piehler, J. Multi-functional DNA Nanostructures That Puncture and Remodel Lipid Membranes Into Hybrid Materials. *Nat. Commun.* **2018**, *9*, 1521.
- (52) Göpfrich, K.; Li, C.-Y.; Mames, I.; Bhamidimarri, S. P.; Ricci, M.; Yoo, J.; Mames, A.; Ohmann, A.; Winterhalter, M.; Stulz, E.; Aksimentiev, A.; Keyser, U. F. Ion Channels Made from a Single Membrane-Spanning DNA Duplex. *Nano Lett.* **2016**, *16*, 4665–4669.
- (53) Göpfrich, K.; Zettl, T.; Meijering, A. E.; Hernández-Ainsa, S.; Kocabay, S.; Liedl, T.; Keyser, U. F. DNA-Tile Structures Induce Ionic Currents through Lipid Membranes. *Nano Lett.* **2015**, *15*, 3134–3148.
- (54) Göpfrich, K.; Li, C. Y.; Ricci, M.; Bhamidimarri, S. P.; Yoo, J.; Gyenes, B.; Ohmann, A.; Winterhalter, M.; Aksimentiev, A.; Keyser, U. F. Large-Conductance Transmembrane Porin Made from DNA Origami. *ACS Nano* **2016**, *10*, 8207–8214.
- (55) Diederichs, T.; Pugh, G.; Dorey, A.; Xing, Y.; Burns, J. R.; Nguyen, Q. H.; Tornow, M.; Tampé, R.; Howorka, S. Synthetic Protein-Conductive Membrane Nanopores Built with DNA. *Nat. Commun.* **2019**, *10*, 5018.
- (56) Langecker, M.; Arnaut, V.; Martin, T. G.; List, S.; Renner, S.; Mayer, M.; Dietz, H.; Simmel, F. C. Synthetic Lipid Membrane Channels Formed by Designed DNA Nanostructures. *Science* **2012**, *338*, 932–936.
- (57) Burns, J. R.; Stulz, E.; Howorka, S. Self-Assembled DNA Nanopores That Span Lipid Bilayers. *Nano Lett.* **2013**, *13*, 2351–2356.
- (58) Burns, J. R.; Al-Juffali, N.; Janes, S. M.; Howorka, S. Membrane-Spanning DNA Nanopores with Cytotoxic Effect. *Angew. Chem., Int. Ed.* **2014**, *53*, 12466–12470.
- (59) Burns, J. R.; Göpfrich, K.; Wood, J. W.; Thacker, V. V.; Stulz, E.; Keyser, U. F.; Howorka, S. Lipid-Bilayer-Spanning DNA Nanopores with a Bifunctional Porphyrin Anchor. *Angew. Chem., Int. Ed.* **2013**, *52*, 12069–12072.
- (60) Douglas, S. M.; Marblestone, A. H.; Teerapittayanon, S.; Vazquez, A.; Church, G. M.; Shih, W. M. Rapid Prototyping of 3D DNA-Origami Shapes with caDNAno. *Nucleic Acids Res.* **2009**, *37*, 5001–5006.
- (61) Yoo, J.; Aksimentiev, A. Molecular Dynamics of Membrane-Spanning DNA Channels: Conductance Mechanism, Electro-Osmotic Transport, and Mechanical Gating. *J. Phys. Chem. Lett.* **2015**, *6*, 4680–4687.
- (62) Seifert, A.; Göpfrich, K.; Burns, J. R.; Fertig, N.; Keyser, U. F.; Howorka, S. Bilayer-Spanning DNA Nanopores with Voltage-Switching between Open and Closed State. *ACS Nano* **2015**, *9*, 1117–1126.
- (63) Maingi, V.; Lelimosin, M. L.; Howorka, S.; Sansom, M. S. Gating-Like Motions and Wall Porosity in a DNA Nanopore Scaffold Revealed by Molecular Simulations. *ACS Nano* **2015**, *9*, 11209–11217.
- (64) Burns, J. R.; Seifert, A.; Fertig, N.; Howorka, S. A Biomimetic DNA-Based Channel for the Ligand-Controlled Transport of Charged

Molecular Cargo Across a Biological Membrane. *Nat. Nanotechnol.* **2016**, *11*, 152–156.

(65) Krishnan, S.; Ziegler, D.; Arnaut, V.; Kapsner, K.; Martin, T. G.; Henneberg, K.; Bausch, A. R.; Dietz, H.; Simmel, F. C. Molecular Transport Through Large-Diameter DNA Nanopores. *Nat. Commun.* **2016**, *7*, 12787.

(66) Renner, S.; Geltinger, S.; Simmel, F. C. Nanopore Translocation and Force Spectroscopy Experiments in Microemulsion Droplets. *Small* **2010**, *6*, 190–194.

(67) Thomsen, R. P.; Malle, M. G.; Okholm, A. H.; Krishnan, S.; Bohr, S. S.-R.; Sørensen, R. S.; Ries, O.; Vogel, S.; Simmel, F. C.; Hatzakis, N. S.; Kjems, J. A Large Size-Selective DNA Nanopore with Sensing Applications. *Nat. Commun.* **2019**, *10*, 5655.

(68) Burns, J. R.; Howorka, S. Structural and Functional Stability of DNA Nanopores in Biological Media. *Nanomaterials* **2019**, *9*, 490.

(69) Debnath, M.; Chakraborty, S.; Kumar, Y. P.; Chaudhuri, R.; Jana, B.; Dash, J. Ionophore Constructed from Non-Covalent Assembly of a G-Quadruplex and Liponucleoside Transports K⁺-Ion Across Biological Membranes. *Nat. Commun.* **2020**, *11*, 429.

(70) List, J.; Weber, M.; Simmel, F. C. Hydrophobic Actuation of a DNA Origami Bilayer Structure. *Angew. Chem., Int. Ed.* **2014**, *53*, 4236–4239.

(71) Ohmann, A.; Göpfrich, K.; Joshi, H.; Thompson, R. F.; Sobota, D.; Ranson, N. A.; Aksimentiev, A.; Keyser, U. F. Controlling Aggregation of Cholesterol-Modified DNA Nanostructures. *Nucleic Acids Res.* **2019**, *47*, 11441–11451.

(72) Henrickson, S. E.; Misakian, M.; Robertson, B.; Kasianowicz, J. J. Driven DNA Transport into an Asymmetric Nanometer-Scale Pore. *Phys. Rev. Lett.* **2000**, *85*, 3057–3060.

(73) Kasianowicz, J. J.; Henrickson, S. E.; Weetall, H. H.; Robertson, B. Simultaneous Multianalyte Detection with a Nanometer-Scale Pore. *Anal. Chem.* **2001**, *73*, 2268–2272.

(74) Wei, R.; Gatterdam, V.; Wieneke, R.; Tampé, R.; Rant, U. Stochastic Sensing of Proteins with Receptor-Modified Solid-State Nanopores. *Nat. Nanotechnol.* **2012**, *7*, 257–263.

(75) Howorka, S.; Siwy, Z. Nanopore Analytics: Sensing of Single Molecules. *Chem. Soc. Rev.* **2009**, *38*, 2360–2384.

(76) Smeets, R. M. M.; Kowalczyk, S. W.; Hall, A. R.; Dekker, N. H.; Dekker, C. Translocation of RecA-Coated Double-Stranded DNA through Solid-State Nanopores. *Nano Lett.* **2009**, *9*, 3089–3095.

(77) Kowalczyk, S. W.; Hall, A. R.; Dekker, C. Detection of Local Protein Structures along DNA Using Solid-State Nanopores. *Nano Lett.* **2010**, *10*, 324–328.

(78) Plesa, C.; Ruitenber, J. W.; Witteveen, M. J.; Dekker, C. Detection of Individual Proteins Bound along DNA Using Solid-State Nanopores. *Nano Lett.* **2015**, *15*, 3153–3158.

(79) Bulushev, R. D.; Marion, S.; Petrova, E.; Davis, S. J.; Maerkl, S. J.; Radenovic, A. Single Molecule Localization and Discrimination of DNA-Protein Complexes by Controlled Translocation Through Nanocapillaries. *Nano Lett.* **2016**, *16*, 7882–7890.

(80) Bell, N. A. W.; Keyser, U. F. Digitally Encoded DNA Nanostructures for Multiplexed, Single-Molecule Protein Sensing with Nanopores. *Nat. Nanotechnol.* **2016**, *11*, 645–651.

(81) Sze, J. Y. Y.; Ivanov, A. P.; Cass, A. E. G.; Edell, J. B. Single Molecule Multiplexed Nanopore Protein Screening in Human Serum Using Aptamer Modified DNA Carriers. *Nat. Commun.* **2017**, *8*, 1552.

(82) Bell, N. A. W.; Keyser, U. F. Specific Protein Detection Using Designed DNA Carriers and Nanopores. *J. Am. Chem. Soc.* **2015**, *137*, 2035–2041.

(83) Plesa, C.; van Loo, N.; Ketterer, P.; Dietz, H.; Dekker, C. Velocity of DNA During Translocation Through a Solid-State Nanopore. *Nano Lett.* **2015**, *15*, 732–737.

(84) Bošković, F.; Zhu, J.; Chen, K.; Keyser, U. F. Monitoring G-Quadruplex Formation with DNA Carriers and Solid-State Nanopores. *Nano Lett.* **2019**, *19*, 7996–8001.

(85) Tippiana, R.; Xiao, W.; Myong, S. G-Quadruplex Conformation and Dynamics Are Determined by Loop Length and Sequence. *Nucleic Acids Res.* **2014**, *42*, 8106–8114.

(86) Chen, K.; Kong, J.; Zhu, J.; Ermann, N.; Predki, P.; Keyser, U. F. Digital Data Storage Using DNA Nanostructures and Solid-State Nanopores. *Nano Lett.* **2019**, *19*, 1210–1215.

(87) Chen, K.; Zhu, J.; Bošković, F.; Keyser, U. F. Nanopore-Based DNA Hard Drives for Rewritable and Secure Data Storage. *Nano Lett.* **2020**, *20*, 3754–3760.

(88) Ishikawa, D.; Suzuki, Y.; Kurokawa, C.; Ohara, M.; Tsuchiya, M.; Morita, M.; Yanagisawa, M.; Endo, M.; Kawano, R.; Takinoue, M. DNA Origami Nanoplate-Based Emulsion with Nanopore Function. *Angew. Chem., Int. Ed.* **2019**, *58*, 15299–15303.

(89) Ohmann, A.; Li, C.; Maffeo, C.; Nahas, K. A.; Baumann, K. N.; Göpfrich, K.; Yoo, J.; Keyser, U. F.; Aksimentiev, A. A Synthetic Enzyme Built from DNA Flips 10⁷ Lipids per Second in Biological Membranes. *Nat. Commun.* **2018**, *9*, 2426.

(90) Gerling, T.; Kube, M.; Kick, B.; Dietz, H. Sequence-Programmable Covalent Bonding of Designed DNA Assemblies. *Sci. Adv.* **2018**, *4*, eaau1157.

(91) Engelhardt, F. A. S.; Praetorius, F.; Wachauf, C. H.; Brüggenthies, G.; Kohler, F.; Kick, B.; Kadletz, K. L.; Nhi Pham, P.; Behler, K. L.; Gerling, T.; Dietz, H. Custom-Size, Functional, and Durable DNA Origami with Design-Specific Scaffolds. *ACS Nano* **2019**, *13*, 5015–5027.

(92) Liu, X.; Zhang, F.; Jing, X.; Pan, M.; Liu, P.; Li, W.; Zhu, B.; Li, J.; Chen, H.; Wang, L.; Lin, J.; Liu, Y.; Zhao, D.; Yan, H.; Fan, C. Complex Silica Composite Nanomaterials Templated with DNA Origami. *Nature* **2018**, *559*, 593–598.

(93) Nguyen, L.; Döblinger, M.; Liedl, T.; Heuer-Jungemann, A. DNA Origami Templated Silica Growth by Sol-Gel Chemistry. *Angew. Chem., Int. Ed.* **2019**, *58*, 912–916.

(94) Nguyen, M.-K.; Nguyen, V. H.; Natarajan, A. K.; Huang, Y.; Ryssy, J.; Shen, B.; Kuzyk, A. Ultrathin Silica Coating of DNA Origami Nanostructures. *Chem. Mater.* **2020**, *32*, 6657–6665.

(95) Anastassacos, F. M.; Zhao, Z.; Zeng, Y.; Shih, W. M. Glutaraldehyde Cross-Linking of Oligolysines Coating DNA Origami Greatly Reduces Susceptibility to Nuclease Degradation. *J. Am. Chem. Soc.* **2020**, *142*, 3311–3315.

(96) Kiviah, J. K.; Linko, V.; Ora, A.; Tiainen, T.; Järvihaavisto, E.; Miikkilä, J.; Tenhu, H.; Nonappa; Kostianen, M. A. Cationic Polymers for DNA Origami Coating – Examining Their Binding Efficiency and Tuning the Enzymatic Reaction Rates. *Nanoscale* **2016**, *8*, 11674–11680.

(97) Praetorius, F.; Kick, B.; Behler, K. L.; Honemann, M. N.; Weuster-Botz, D.; Dietz, H. Biotechnological Mass Production of DNA Origami. *Nature* **2017**, *552*, 84–87.

(98) Ramakrishnan, S.; Ijäs, H.; Linko, V.; Keller, A. Structural Stability of DNA Origami Nanostructures under Application-Specific Conditions. *Comput. Struct. Biotechnol. J.* **2018**, *16*, 342–349.

(99) Bila, H.; Kurisinkal, E. E.; Bastings, M. M. C. Engineering a Stable Future for DNA-Origami as a Biomaterial. *Biomater. Sci.* **2019**, *7*, 532–541.